

Estimation of Spectral Distribution of Scene Illumination from a Single Image

Cheol-Hee Lee†

Department of Computer Engineering, Kyungwoon Univ., Gumig, Kyungbuk, Korea

Byung-Joon Moon

Optics & Digital Imaging Development Division, Samsung Techwin Co., Ltd., Suwon, Kyungki, Korea

Ho-Young Lee, Eui-Yoon Chung, and Yeong-Ho Ha▲

School of Electronic and Electrical Engineering, Kyungpook National Univ., Taegu, Korea

This article proposes an illuminant estimation algorithm that estimates the spectral power distribution of an incident light source from a single image. The proposed illumination recovery procedure has two phases. First, the surface spectral reflectances are recovered. In this case, the surface spectral reflectances recovered are limited to the maximum achromatic region (MAR) which is the most achromatic and highly bright region of an image, after applying intermediate color constancy process using a modified gray-world algorithm. Next, the surface reflectances of the maximum achromatic region are estimated using the principal component analysis method along with a set of given Munsell samples. Second, the spectral distribution of reflected lights of MAR is selected from the spectral database. That is, a color difference is compared between the reflected lights of the MAR and the spectral database, which is the set of reflected lights built by the given Munsell samples and a set of illuminants. Then the closest colors from the spectral database are selected. Finally, the illuminant of an image can be calculated dividing the average spectral distributions of reflected lights of MAR by the average surface reflectances of the MAR. In order to evaluate the proposed algorithm, experiments with artificial and real captured color-biased scenes were performed and numerical comparison examined. The proposed method was effective in estimating the spectral distribution of the given illuminants under various illuminants and scenes without white points.

Journal of Imaging Science and Technology 44: 308–320 (2000)

Introduction

The human visual system (HVS) is able to assign roughly constant colors to objects under varying illumination by discounting the illuminants. This adaptability of the HVS enables the accurate identification of objects in diverse visual environments. However, electric cameras have no such adaptation mechanisms, therefore, captured images can exhibit substantial differences according to the incidental light. In order to obtain a similar color appearance for scenes in an electronic camera, illuminant estimation is required so that the stability of surface reflectance can be recovered. This illuminant or surface reflectance decoupling from the reflected colors of scene is called color constancy.

Color constancy in the HVS has been studied by many color researchers, yet this decoupling process is generally an ill-posed problem.^{1,2} In the case of a color con-

stancy approach based on a linear model,³ given an RGB-format image including N surfaces, $3N + 3$ descriptors are required to decouple an illuminant and surfaces. However, a trichromatic camera system has just $3N$ quantum catch data.²

As a basic theory in conjunction with a unique recovery for lights and surfaces, D'Zmura and his colleagues presented a criterion for determining this unique recovery according to the number of unknown lights and surface parameters based on the linear model of Maloney and Wandell.^{1,3,4} However, multiple images of a scene with different illuminants are required for exact color recovery. In order to overcome this mismatch between known and unknown descriptors of scenes, additional assumptions have been developed to estimate the surfaces or illuminants of the scenes.

The basic assumption for surfaces is the gray-world algorithm that the average spectral reflectance of all the surfaces in the image is gray. Another assumption for surfaces is the brightest surface method, which is one of the most simple and widely used color constancy algorithms. In this method, the brightest surface of an image is assumed as a uniform perfect reflector.³ As a result, the scene illuminant can be decoupled directly. This article proposes an effective illuminant estimation

Invited paper; Original manuscript received March 8, 1999

† Student member; ▲ IS&T Member

Supplemental materials—Figures 5, 6, 7, 8, 9, 10 and 11 can be found on the IS&T website (www.imaging.org) for a period of no less than 2 years from the date of publication.

©2000, IS&T—The Society for Imaging Science and Technology

method combining the brightest surface method⁵ and modified gray-world assumption.⁶ In order to calculate the brightest surface from color-biased images discounting illuminants, a modified gray-world assumption was applied. By using modified gray-world assumption, the influence of illumination in the input image is partially eliminated for each channel. Then, the neutralized image is exploited to obtain the maximum achromatic region (MAR). After choosing the MAR, the surface spectral reflectances of the MAR are calculated by the principal component analysis.⁷

Next, the spectral distributions of reflected lights, which are the closest ones to the colors of the corresponding MAR, are then identified from a set of reflected lights, built by the given set of illuminants and surface reflectances of the Munsell samples. Therefore, color-biased images can be recovered accurately through dividing the spectral power distribution of the reflected lights by the surface spectral reflectance of the MAR.

Linear Models

Linear models have been widely used to approximate three components in the color perception of the HVS. With the use of linear models, illuminants, surface reflectances and the response of receptors of the HVS can all be represented as weighted sums of basis functions:

$$E(\lambda) \cong \sum_{i=1}^m e_i E_i(\lambda) \quad (1)$$

where $E_i(\lambda)$ are basis functions used to approximate the spectral measurements of the illuminants, e_i are the illuminant coefficients. Judd collected the spectral power distributions of 622 samples of daylight to generate 1 mean and 4 basis vectors for the spectral representation of daylight illuminants.⁸

Due to smoothness of surface spectral reflectances in the visible wavelength range, a variety of surfaces can be approximated by a fixed set of basis functions, $R_j(\lambda)$ and surface coefficients, r_j as shown below

$$R(\lambda) \cong \sum_{j=1}^n r_j R_j(\lambda). \quad (2)$$

Given an illuminant, $E(\lambda)$ reflected light to a surface with spectral reflectance of $R(\lambda)$ can be represented by the linear models as shown below

$$L(\lambda) \cong \sum_{i=1}^m \sum_{j=1}^n e_i r_j E_i(\lambda) R_j(\lambda). \quad (3)$$

Finally, the quantum catch data caught by the human eye can be represented as photoreceptor responses to reflected lights as shown below

$$q_k \cong \sum_{i=1}^m \sum_{j=1}^n e_i r_j a_{ijk}, \quad k = 1 \text{ to } p, \quad a_{ijk} = \int Q_k(\lambda) E_i(\lambda) R_j(\lambda) d\lambda. \quad (4)$$

where $E_i(\lambda)$ and $R_j(\lambda)$ are the constants for the images. Accordingly, color recovery in a trichromatic visual system means decoupling e_i and r_j from the quantum catch data, q_k . However, color recovery in a trichromatic visual system has certain constraints because the number of known parameters is lower than the number of

unknown parameters. For a surface, the number of known parameters is 3, yet for an illuminant and surface reflectance 6 coefficients are still unknown. As a result, a direct linear solution to identify the illuminants or surface reflectances using only three quantum catch data is impossible.

To overcome this mismatch, various color constancy algorithms have been introduced including the gray-world assumption and the brightest surface method. The former is based on the assumption that the average spectral reflectance of an image is gray, and the latter infers that the brightest surface of an image includes enough information about the illuminant of a scene. This prior information on the surface reflectance or illuminants of a scene is then used to recover the remaining illuminants or surface reflectances.

The proposed approach is based on the brightest surface method. However, the conventional brightest surface method cannot recover correctly the illuminant of a scene that has no white points in the image, because, the brightest surface method solves the mismatch on the assumption that white points can estimate illuminants of a scene. As mentioned earlier, the current study is based on the assumption that the brightest region of an image includes sufficient information on the illuminants of a scene. However, we consider that the brightest region in real image cannot be assumed as a uniform reflector. Therefore, our approach can be applied to images without white patches.

In our study, we define the MAR region, which is the maximum achromatic region of an image. For MAR, the reflected light and corresponding surface reflectances are calculated. Then, the illuminants of the scene are finally estimated by using the calculated reflected lights and surface reflectances.

Estimation Method of Illuminants of Scenes Estimation of the Surface Spectral Reflectance of MAR

As mentioned before, our approach based on the assumption that if there is a maximum surface reflectance, the maximum spectral power distribution of light reflected from surfaces with an illuminant $E(\lambda)$ will be

$$L_{\max}(\lambda) = E(\lambda) R_{\max}(\lambda). \quad (5)$$

If an image is colorful, the maximum value of the spectral distribution of light reflected from the maximum surface reflectance could be assumed to be an estimation of $L_{\max}(\lambda)$. As a first step, $L_{\max}(\lambda)$ is obtained from the image. Thereafter, the estimation of the illuminant for an input image can be calculated using Eq. 6.

$$\hat{E}(\lambda) = \frac{\hat{L}_{\max}(\lambda)}{R_{\max}(\lambda)} \quad (6)$$

Basically, our assumption for Eqs. 5 and 6 is same as in Cheng's approach.⁹ $R_{\max}(\lambda)$ is very important for obtaining an exact description of an illuminant, yet in Cheng's approach, $R_{\max}(\lambda)$ is a fixed value deduced from the assumption that the lights reflected from $R_{\max}(\lambda)$ have a maximum tristimulus value, $q = [111]^T$. Accordingly, $R_{\max}(\lambda)$ is calculated using a fixed spectral distribution of the reflected light with constant weighting vector and fixed spectral distribution of D65.⁹ As a result, $R_{\max}(\lambda)$ and the estimated $\hat{E}(\lambda)$ are not adaptive for an image. Plus the estimated $\hat{E}(\lambda)$ cannot be optimal for images that do not include ideal white.

In the proposed method, the $R_{\max}(\lambda)$ and $L_{\max}(\lambda)$ of an image are simultaneously estimated from the same surface of the image. Therefore, the application of the proposed algorithm can extend to images that do not include ideal white because $R_{\max}(\lambda)$ is not required to become a constant spectral function or uniform spectral function.

As the first approach, to identify the MAR, a modified version of the gray world assumption technique of Buchsbaum,⁶ an intermediate color constancy approach, is applied to partially eliminate the influence of illumination before MAR search. In Eq. 7, the average lightness value of each channel indicates the average reflectance at each channel. In the case of illumination variation, the average lightness value of each channel will change.

Hence, normalization using the average of each channel removes the illumination variation and R_{gray} , G_{gray} , and B_{gray} were utilized as the denominators in Eq. 7, thereby implying a 128 gray value. This is based on the assumption that the average of all the surfaces in an image is that of a middle-gray. Therefore, after applying Eq. 7, the average of each channel in an image is mapped to a middle-gray.

$$\begin{bmatrix} R'(i, j) \\ G'(i, j) \\ B'(i, j) \end{bmatrix} = \begin{bmatrix} \frac{R_{gray}}{R_m} & 0 & 0 \\ 0 & \frac{G_{gray}}{G_m} & 0 \\ 0 & 0 & \frac{B_{gray}}{B_m} \end{bmatrix} \begin{bmatrix} R(i, j) \\ G(i, j) \\ B(i, j) \end{bmatrix}, \quad (7)$$

$$R_m = E\{R(i, j)\}, \quad G_m = E\{G(i, j)\}, \quad B_m = E\{B(i, j)\}$$

$$\text{if } |C_k(i, j) - C_l(i, j)| \text{ for } k, l = R, G, B \text{ and } k \neq l > 10$$

where C_k are the color vectors, which have R, G, and B components. When the channel means are calculated for each channel of images, gray colors or dark colors are omitted to avoid saturation of image due to small magnitude of averages in the normalization process. After scaling using the modified gray world assumption, the chromatic images are transformed into Yc_bC_r color space to find MAR as shown in Eq. 8.

$$\begin{aligned} Y &= 0.299R' + 0.587G' + 0.114B' \\ C_b &= 0.577(B' - Y) \\ C_r &= 0.730(R' - Y). \end{aligned} \quad (8)$$

Then, the MAR is determined by selecting the minimum chromatic points in an image. In Eq. 9, the local chromatic component, $C(i, j)$, is the euclidean sum of C_b and C_r in a 7×7 block.

$$\text{if } Y(i, j) > \text{Threshold}$$

$$C(i, j) = \sum_{i=1}^7 \sum_{j=1}^7 \sqrt{C_b(i, j)^2 + C_r(i, j)^2} \quad (9)$$

The 7×7 block size was empirically determined to avoid the selection of impulse noise points in the MAR search. In addition, in order to select bright points, the range of minimum chromatic points is limited to a re-

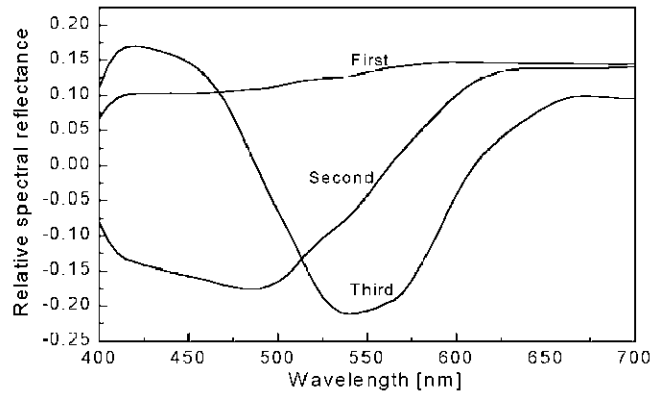


Figure 1. Principal components for 1269 Munsell chips

gion where the luminance channel, Y is higher than 90% of that of the input image.

After determining the MAR, the pixels of the central 3×3 block in the selected region are converted into XYZ values in order to apply the principal component analysis method as follows.

$$\begin{bmatrix} X \\ Y \\ Z \end{bmatrix} = \begin{bmatrix} 0.588 & 0.179 & 0.183 \\ 0.290 & 0.606 & 0.105 \\ 0.000 & 0.068 & 1.021 \end{bmatrix} \begin{bmatrix} R \\ G \\ B \end{bmatrix} \quad (10)$$

In order to produce principal components (basis functions) of surface reflectance, 1269 chips from the *Munsell Book of Color* were exploited. The Munsell spectra were obtained from the Information Technology Dept., Lappeenranta Univ. of Technology.¹⁰ Thereafter, three basis functions of these spectra were generated by a principal component analysis. Table I show the three basis functions calculated using 1269 Munsell surface spectral reflectances.

Using the principal component vectors, the surface spectral reflectances of the object can be expressed as a linear combination as follows

$$R(\lambda) \cong \bar{R}(\lambda) + \sum_{i=1}^3 \alpha_i u_i = \bar{R}(\lambda) + [u_1 \ u_2 \ u_3] \begin{bmatrix} \alpha_1 \\ \alpha_2 \\ \alpha_3 \end{bmatrix}. \quad (11)$$

where, $\bar{R}(\lambda)$ is the average of surface reflectances. u_i are the principal components and α_i are the corresponding coefficients to u_i . Figure 1 illustrates the three principal components utilized in this study. In Eq. 9, the 9 surface coefficients of the selected 9 pixels, that is MAR in an image, can be calculated by Eqs. 12 and 13.

$$\begin{bmatrix} X \\ Y \\ Z \end{bmatrix} \cong \begin{bmatrix} \bar{X} \\ \bar{Y} \\ \bar{Z} \end{bmatrix} + \begin{bmatrix} X_1 & X_2 & X_3 \\ Y_1 & Y_2 & Y_3 \\ Z_1 & Z_2 & Z_3 \end{bmatrix} \begin{bmatrix} \alpha_1 \\ \alpha_2 \\ \alpha_3 \end{bmatrix} \quad (12)$$

where \bar{X} , \bar{Y} , and \bar{Z} are the tristimulus values to the averaged spectral of 1269 Munsell samples and X_i , Y_i , and Z_i ($i = 1, 2, 3$) are the tristimulus values for the corresponding principal components. Accordingly, surface

TABLE I. Principal Components of 1269 Munsell Surface Spectral Reflectances

Wavelength (nm)	Principal Components			Wavelength (nm)	Principal Components		
	First	Second	Third		First	Second	Third
400	0.070755	-0.083613	0.113443	405	0.087898	-0.108063	0.143397
410	0.098271	-0.124223	0.160889	415	0.102981	-0.133032	0.168006
420	0.104293	-0.137806	0.169081	425	0.104365	-0.141468	0.167358
430	0.104581	-0.144279	0.164634	435	0.104606	-0.147598	0.161336
440	0.104698	-0.150778	0.157645	445	0.104457	-0.154055	0.152153
450	0.104421	-0.15653	0.145215	455	0.104785	-0.159577	0.136555
460	0.105254	-0.162504	0.125585	465	0.106075	-0.165872	0.110818
470	0.107271	-0.16894	0.092882	475	0.108341	-0.171469	0.068690
480	0.109268	-0.173412	0.042419	485	0.110084	-0.174106	0.012311
490	0.111129	-0.172877	-0.014962	495	0.112652	-0.169702	-0.042122
500	0.114558	-0.163887	-0.065579	505	0.117100	-0.15396	-0.089916
510	0.119606	-0.141573	-0.114631	515	0.121926	-0.127038	-0.14233
520	0.123374	-0.114032	-0.166917	525	0.124258	-0.10148	-0.187886
530	0.125093	-0.091306	-0.201434	535	0.126212	-0.080903	-0.20971
540	0.127606	-0.07022	-0.211814	545	0.129983	-0.056724	-0.210353
550	0.132778	-0.041418	-0.207352	555	0.135688	-0.022569	-0.20326
560	0.138152	-0.006184	-0.196809	565	0.139548	0.010737	-0.191516
570	0.140794	0.023813	-0.180599	575	0.142233	0.037646	-0.163478
580	0.143405	0.050663	-0.142371	585	0.144543	0.06498	-0.116766
590	0.145318	0.078124	-0.091873	595	0.145752	0.091273	-0.065083
600	0.145809	0.102270	-0.041499	605	0.145584	0.112179	-0.01827
610	0.145388	0.120117	-0.000218	615	0.144970	0.126771	0.016349
620	0.144576	0.131288	0.028687	625	0.144326	0.134932	0.040147
630	0.144491	0.137492	0.049636	635	0.144311	0.138869	0.058908
640	0.143968	0.139296	0.067144	645	0.143996	0.139746	0.076000
650	0.143885	0.139758	0.083390	655	0.143616	0.139070	0.090317
660	0.143578	0.138975	0.094866	665	0.143698	0.139034	0.098621
670	0.143049	0.138491	0.099073	675	0.143235	0.139299	0.099418
680	0.142787	0.139483	0.098544	685	0.142939	0.139991	0.097979
690	0.142474	0.139940	0.096370	695	0.142933	0.140849	0.095812
700	0.142838	0.141018	0.095371				

coefficients $\alpha_i(i = 1,2,3)$ are given by

$$\begin{bmatrix} \alpha_1 \\ \alpha_2 \\ \alpha_3 \end{bmatrix} = \begin{bmatrix} X_1 & X_2 & X_3 \\ Y_1 & Y_2 & Y_3 \\ Z_1 & Z_2 & Z_3 \end{bmatrix}^{-1} \left(\begin{bmatrix} X \\ Y \\ Z \end{bmatrix} - \begin{bmatrix} \bar{X} \\ \bar{Y} \\ \bar{Z} \end{bmatrix} \right) \quad (13)$$

Therefore, the 9 surface reflectances of the MAR can be estimated using above surface coefficients, the spectral mean of Munsell, and principal components as shown in Eq. 11.

Determination of Spectral Power Distributions of the Reflected Lights on MAR

The proposed approach for estimating the illuminants of a scene has two phases. First, the surface spectral reflectance of the MAR is estimated. Next the spectral distribution of the reflected light of the MAR is determined. In our study, the 1269 samples of *Munsell Book of Color* and 6 illuminants (A, C, D65, D50, Green, and Yellow) were used to compose the set of reflected lights. Figure 2 shows the spectral power distributions of the 6 illuminants.

The same 1269 Munsell spectra were utilized for building the principal components for the surface spectral reflectances and constructing the spectra set of reflected lights. The Munsell spectra were multiplied by 6

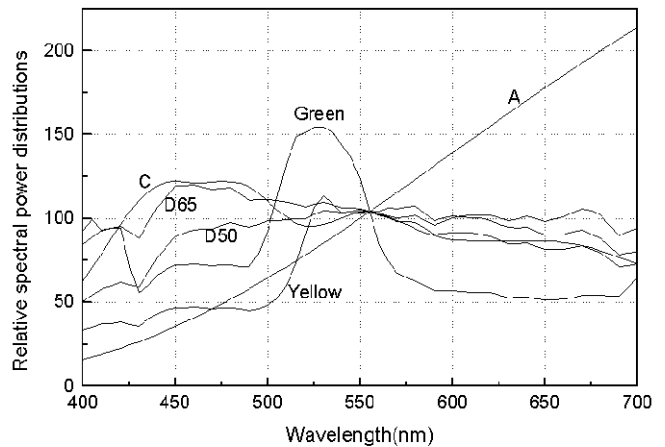


Figure 2. Spectral power distributions of the 6 illuminants used in constructing the spectral database of the reflected lights.

illuminants to generate a set of spectral power distributions of reflected lights from 400 ~ 700 nm at 5 nm intervals. Hereafter, this set of spectra is referred to as the spectral database. The chromaticity diagram of the spectral database is shown below.

The colors of the MAR are then compared with the spectral database to find the closest spectral data. For a comparison in uniform color space, the 9 colors of the MAR and the spectral data in the spectral database can

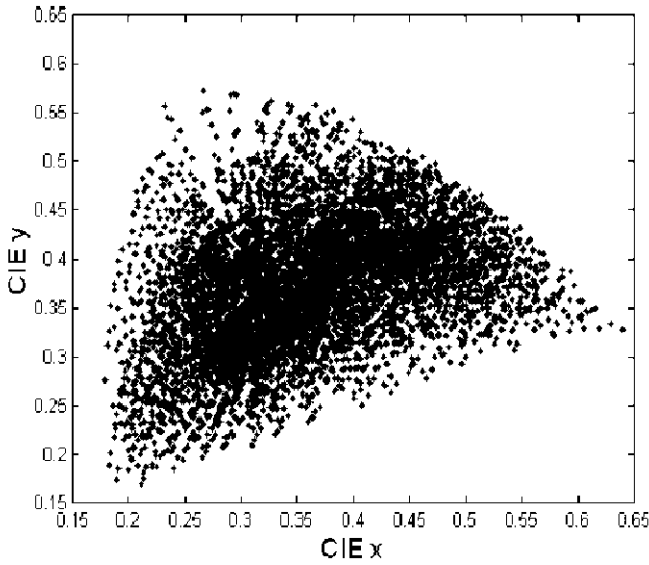


Figure 3. Chromaticity diagram of the spectral database (1269 × 6).

be transformed into $L^*a^*b^*$ vectors as below:

$$\begin{aligned}
 L^* &= 116f(Y/Y_n) - 16 \\
 a^* &= 500[f(X/X_n) - f(Y/Y_n)] \\
 b^* &= 200[f(Y/Y_n) - f(Z/Z_n)] \\
 f(\omega) &= \begin{cases} \omega^{1/3} & \omega > 0.008856 \\ 7.787\omega + 16/116 & \omega \leq 0.008856 \end{cases} \quad (14)
 \end{aligned}$$

Then, the criterion for selecting the best matching spectra is as follows:

$$\Delta E = \sqrt{(L_{MAR} - L_d)^2 + (a_{MAR} - a_d)^2 + (b_{MAR} - b_d)^2} \quad (15)$$

where, L_{MAR} denotes the lightness of a MAR color in CIELAB color space and L_d means the lightness of a sample of spectral database in CIELAB metric. Using Eq. 15, 9 spectral distributions of the lights reflected from the MAR are selected from the spectral database. Finally, the selected spectral data are divided by the corresponding surface spectral reflectances of the MAR and averaged to estimate the spectral distribution of the illuminant. A flowchart of the proposed algorithm is shown in Fig. 4.

Recovering Colors

After estimating the spectral power distribution of the illuminant, the colors of images with chromatic illuminants can be recovered by matrix transformation. There are three distinct classes of receptors in a trichromatic visual system. Therefore, the response of a class- k receptor is:

$$q_k = \sum_{j=1}^3 [r_j \int Q_k(\lambda)E(\lambda)R_j(\lambda)d\lambda]. \quad (16)$$

If the illuminant of a scene, $E(\lambda)$ is estimated, Eq. 16 can be expressed in matrix form

$$\begin{bmatrix} X \\ Y \\ Z \end{bmatrix} = \begin{bmatrix} b_{11} & b_{12} & b_{13} \\ b_{21} & b_{22} & b_{23} \\ b_{31} & b_{32} & b_{33} \end{bmatrix} \begin{bmatrix} r_1 \\ r_2 \\ r_3 \end{bmatrix} \quad (17)$$

or

$$\mathbf{q} = \mathbf{B}\mathbf{r} \quad (18)$$

where

$$b_{kj} = \int Q_k(\lambda)E(\lambda)R_j(\lambda)d\lambda. \quad (19)$$

Assume that the column vector of the tristimulus values of a surface with the original illuminant is \mathbf{q}_{orig} and the transformation matrix is \mathbf{B}_{orig} . From Eq. 19,

$$\mathbf{r} = \mathbf{B}_{orig}^{-1}\mathbf{q}_{orig}. \quad (20)$$

Therefore, the recovered image with the CIE standard illuminant D65 can be calculated by

$$\mathbf{q}_{D65} = \mathbf{B}_{D65}\mathbf{r} = (\mathbf{B}_{D65}\mathbf{B}_{orig}^{-1})\mathbf{q}_{orig}. \quad (21)$$

Finally, the neutral image in RGB-format can be obtained by an inverse transformation of Eq. 10 as shown below.

$$\begin{bmatrix} R \\ G \\ B \end{bmatrix} = \begin{bmatrix} 1.971 & -0.549 & -0.297 \\ -0.954 & 1.936 & -0.027 \\ 0.064 & -0.129 & 0.982 \end{bmatrix} \begin{bmatrix} X \\ Y \\ Z \end{bmatrix} \quad (22)$$

Results and Discussion

The proposed method was simulated using artificial color-biased images and digital camera images captured under chromatic light sources. First, to produce artificial color-biased images, the RGB input images were converted to multi-spectral images using linear model and principal components. Here, it was assumed that the scene illuminant of the original image was D65. Then, piecewise multiplication with known chromatic illuminants produced the artificial color-biased images. A, C, D50, green, and yellow were utilized as the chromatic illuminants. Each chromatic illuminant has 61 samples and spans 400 ~ 700 nm at 5 nm intervals. 1269 × 6 spectra were used as the spectral database. Figures 5 through 11 illustrate the results for the artificial color-biased images with A, green, and yellow.

As shown in Figs. 5 through 11, the original image in RGB-format was biased by the chromatic illuminants, A, green, and yellow, respectively. The illuminants of the artificial color-biased images were then estimated using the proposed and Cheng's *Maximum Tristimulus Value* methods, and these estimated scene illuminants for each image facilitated the recovery of a neutral image under D65. As previously mentioned, in the proposed method, $R_{max}(\lambda)$ is adaptive for input images and does not need to be a constant spectral function or uniform surface spectral function. Therefore, the proposed illuminant estimation method is more adaptive than

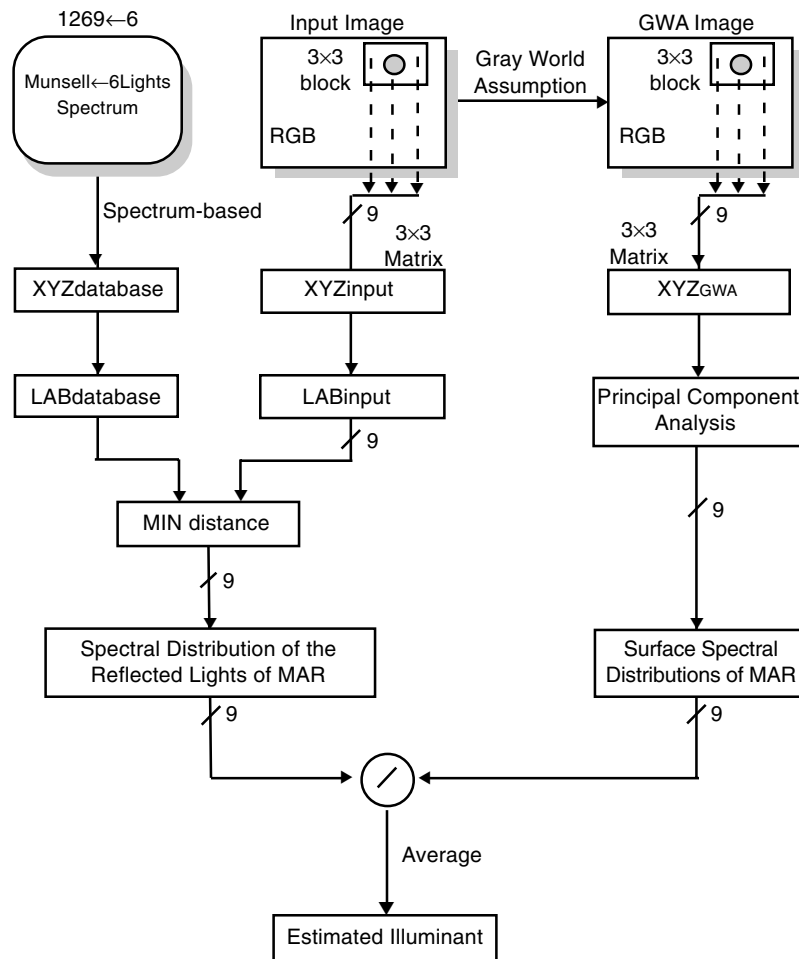


Figure 4. Flowchart of the proposed algorithm.

Cheng's method in illuminant estimation. Table II shows color difference comparisons for the test images of Figs. 5 through 11.

Second, an experiment using real color-biased images was performed. In order to generate the real color-biased images, the *Macbeth Color-Checker* was captured in a *Macbeth* viewing booth with changing light sources. A Sony DSC-D700 digital camera was used and its camera characteristics were fixed to avoid any self-compensation of the scene illuminants. The non-compressed TIFF-format images were converted into RAW-format RGB images using the image manipulation package, Paint Shop Pro 5.0 and then used as the test images.

Inc A, TL84, and Horizon light sources were utilized as the chromatic light sources in the *Macbeth* viewing booth. Then, the illuminants of the real color-biased images were estimated using the proposed method and the images were recovered into a neutral image under D65 using the estimated illuminants. Finally, results images were compared with the captured image under D65 as shown in Figs. 8 through 11.

The results confirmed that the proposed method could effectively estimate the illuminants under different illumination conditions. In particular, the proposed method functioned well in the simulations using specular surfaces that were not considered in Cheng's approach. However, the illuminant estimation for the red-biased image was incorrect in the long wavelength region. As a result, this mismatch was analyzed by in-

TABLE II. Color Difference Comparison Between Cheng and Proposed Method

Image	Cheng	Proposed
Inc A	0.0082	0.0024
C	3.2968×10^{-4}	1.9873×10^{-6}
Green	0.0024	3.4999×10^{-6}
Yellow	0.0010	6.3392×10^{-6}

vestigating the selected spectra in relation to the lights reflected from the MAR. In the case of illuminant A, the selected spectra from the spectral database can include a few reflected lights, illuminated by different lights. Accordingly, the slope in the long wavelength region did not follow the curve of the original illuminant. This phenomenon can be described in three ways.

First, loss of the red signal when capturing an image may be a reason. An Inc A or Horizon illuminant has a large spectral power distribution in the long wavelength part. Therefore, the captured red signal of an image may exceed the maximum gray level. For reproduction on a monitor, the red signal then should be clipped before saving the image in the camera. Accordingly, a color-biased image caused by Inc A or Horizon will result in lost data in the red channel. As a result, the estimated illuminants will show little difference from the known or the real illuminants in a long wavelength part.



(a)



(b)

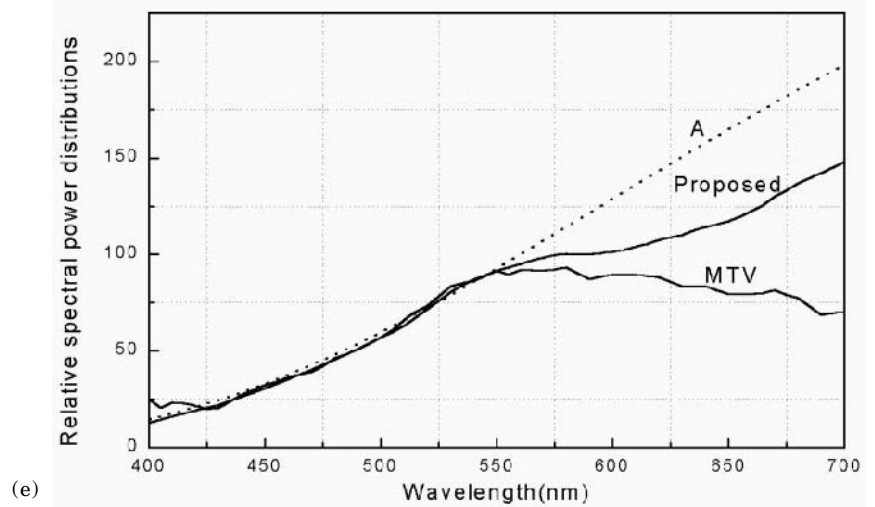


(c)



(d)

Figure 5. Recovered images for illuminant A and the spectral power distribution of estimated illuminants. (a) original image, (b) color-biased image by the illuminant A, (c) recovered image by Cheng's *maximum-tristimulus value (MTV)* method, (d) recovered image by the proposed method, (e) estimated illuminants A by Cheng's method and proposed method. (dot: original spectral, solid: estimated spectral).



(e)



(a)



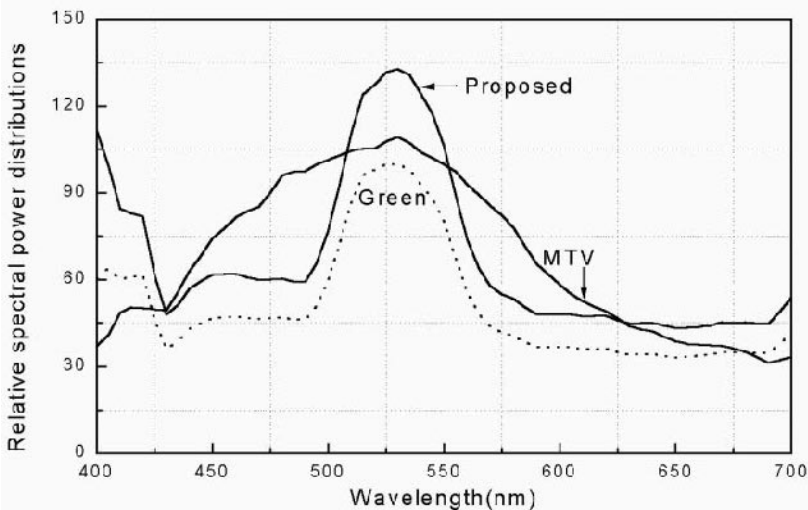
(b)



(c)



(d)



(e)

Figure 6. Recovered images for the green illuminant and the spectral power distribution of estimated illuminants. (a) original image, (b) color-biased image by the illuminant green, (c) recovered image by Cheng's *maximum-tristimulus value*(MTV) method, (d) recovered image by the proposed method, (e) estimated illuminants green by Cheng's method and by proposed method. (dot: original spectral, solid: estimated spectral).



(a)



(b)

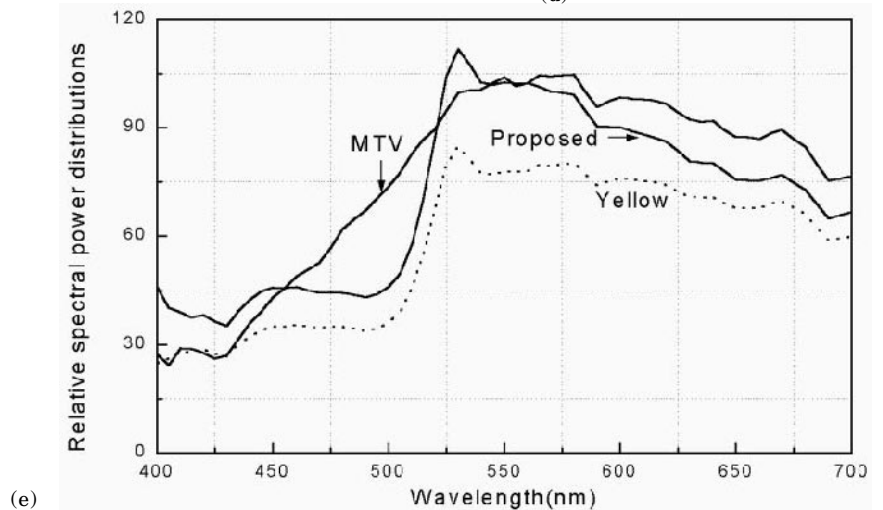


(c)



(d)

Figure 7. Recovered images for the illuminant yellow and the spectral power distribution of estimated illuminants. (a) original image, (b) color-biased image by the illuminant yellow, (c) recovered image by Cheng's *maximum-tristimulus value*(MTV) method, (d) recovered image by the proposed method, (e) estimated illuminants yellow by Cheng's method and by proposed method. (dot: original spectral, solid: estimated spectral)



(e)



(a)



(a)



(b)



(b)



(c)



(c)

Figure 8. Experiment for *Macbeth Color-Checker* under Inc A in the *Macbeth* viewing booth. (a) captured image under D65 in the *Macbeth* viewing booth, (b) captured image under Inc A in the *Macbeth* viewing booth, and (c) recovered image of (b) by the proposed method.

Figure 9. Experiment for *Macbeth Color-Checker* under Horizon in the *Macbeth* viewing booth. (a) captured image under D65 in the *Macbeth* viewing booth, (b) captured image under Horizon in the *Macbeth* viewing booth, and (c) recovered image of (b) by the proposed method.



(a)



(b)



(c)

Figure 10. Experiment for *Macbeth Color-Checker* under TL84 in the *Macbeth* viewing booth. (a) captured image under D65 in the *Macbeth* viewing booth, (b) captured image under TL84 in the *Macbeth* viewing booth, and (c) recovered image of (b) by the proposed method.



(a)



(b)



(c)



(d)



(e)

Figure 11. Experiment for *Macbeth Color-Checker* with specular surfaces under Inc A and Horizon in the *Macbeth* viewing booth. (a) captured image under D65 in the *Macbeth* viewing booth, (b) captured image under A in the *Macbeth* viewing booth, (c) recovered image of (b) by the proposed method, (d) captured image under Horizon in the *Macbeth* viewing booth, and (e) recovered image of (d) by the proposed method.

However, in spite of the data loss due to the saturation of the red signal, mostly original A-biased reflected lights can be chosen from the spectral database. Therefore, the estimated light will be similar to the original red illuminant. Accordingly, color recovery using an estimated illuminant from images which have lost the red signal, produces a blue cast in the scene, as shown in the white patch of Fig. 8(c) and 9(c), and in the watch of Fig. 11(e). Furthermore, it appears more clearly in color recovery from horizon-biased images than in color recovery from Inc A-biased images.

Second, it is a problem related to the dimensional size of the selected minimum color spectra. Namely, 61 samples of spectral data were represented as the 3-dimensional data of CIE $L^*a^*b^*$. In this process, a substantial amount of information on the illuminant color can be lost.

Third, the size of the spectral database also influences the results. A small sample set for reflected lights can create big color differences between the colors of the spectral database. Therefore, if one or two colors, illuminated by different illuminants, are included in the selected spectra, this has a significant influence on the curve of the averaged spectra selected from the spectral database. In particular, illuminant A is a highly red-biased curve. Accordingly, the sample space between the red-colors in the spectral database includes more voids than the sample spaces between other colors. When several spectra were chosen that were illuminated by different illuminants, the error was greater.

Therefore, to improve the accuracy of illuminant estimation, a bigger spectral database is required.

Conclusions

This article proposed an effective illuminant estimation method combining the brightest surface method and modified gray world assumption. A modified gray world algorithm was adopted to calculate the brightest surface from color-biased images discounting illuminants. The use of the modified gray world assumption enabled the partial elimination of the influence of illumination in the input images for each channel. Thereafter, the neutralized image was exploited to obtain the maximum achromatic region (MAR). After determining the MAR, the surface spectral reflectances of the MAR were calculated using a principal component analysis.

Next, the spectral distributions of the reflected lights, the closest ones to the colors of the corresponding MAR, were identified from the spectral database. Then, the color-biased images were recovered through dividing the spectral power distribution of the reflected lights by the surface spectral reflectance of the MAR. Finally, the estimated spectral power distributions of the scene illuminants were averaged to generate the illuminant for the input color-biased image.

Based on the results, the proposed method produced good estimates for various illuminants. However, the results of the red-biased image were less accurate, therefore, further research is required to consider the saturation of the red channel in image capture and the size of the spectral database.

An illuminant has a strong influence on determining the color appearance of an object. Therefore, the estimation of the scene illuminant of an image in a spectral domain can be applied to a variety of applications including a color appearance model. ▲

Acknowledgment. This research was supported by KOREA MOST (Ministry of Science & Technology) under contract number G17-A-08.

References

1. L. T. Maloney and B. A. Wandell, Color constancy: A method for recovering surface spectral reflectance, *J. Opt. Soc. Am. A* **3**, 29–33 (1986).
2. M. D'Zmura and G. Iverson, Color constancy I. Basic theory of two-stage linear recovery of spectral descriptions for lights and surfaces, *J. Opt. Soc. Am. A* **10**, 2148–2165 (1993).
3. B. A. Wandell, *Foundations of Vision*, Sinauer Associates Inc., Sunderland, Massachusetts, 1995, pp. 296–308.
4. M. D'Zmura, Color constancy: Surface color from changing illumination, *J. Opt. Soc. Am. A* **9**, 490–493 (1992).
5. J. J. McCann, J. A. Hall and E. H. Land, Color Mondrian Experiments: The study of average spectral distributions, *J. Opt. Soc. Am. A* **67**, 1380 (1977).
6. G. Buchsbaum, A spatial processor model for object color perception, *J. Franklin Inst.* **310**, 1–26 (1980).
7. M. J. Vhrel and H. J. Trussel, Color correction using principal components, *Color Res. Appl.* **17**, 328–338 (1992).
8. D. B. Judd, D. L. Macadam, and G. Wyszecki, Spectral distribution of typical daylight as a function of correlated color temperature, *J. Opt. Soc. Am. A* **54**, 1031–1042 (1964).
9. F. H. Cheng, Recovering colors in an image with chromatic illuminant, *IEEE Trans. Imaging Processing* **7**, 1524–1533 (1998).
10. http://www.it.lut.fi/research/color/lutcs_database.html.